

Topotactic transformation and dehydration of the zeolite gismondine to a novel Ca feldspar structure

EVA WADOSKI-ROMEIJN AND THOMAS ARMBRUSTER*

Mineralogical Crystallography, Institute of Geological Sciences, University of Bern, Freiestrasse 3, CH-3012 Bern, Switzerland

ABSTRACT

Temperature-dependent single-crystal X-ray data were collected on gismondine (**GIS**) $\text{Ca}_4(\text{Al}_8\text{Si}_8\text{O}_{32})\cdot 18\text{H}_2\text{O}$ from Rio Pian del Foco, Genova province, Italy, in steps of 25 °C up to 600 °C. At room temperature, gismondine has space group $P2_1/c$ with $a = 10.0214(1)$, $b = 10.5997(1)$, $c = 9.8327(1)$ Å, $\beta = 92.363(1)^\circ$, $V = 1043.58(2)$ Å³. This structure remained stable up to 50 °C. The dehydration behavior then divided into two different pathways depending on the sample. In the more frequent path I, the LT $P2_12_12_1$ structure (phase B) $\text{Ca}_4(\text{Al}_8\text{Si}_8\text{O}_{32})\cdot 12\text{H}_2\text{O}$ [$a = 13.6801(8)$, $b = 10.4670(6)$, $c = 13.8667(9)$ Å, $V = 1985.6(2)$ Å³] formed at 75 °C. The orthorhombic structure has a doubled volume relative to the monoclinic room-temperature structure. At 150 °C the HT $P2_12_12_1$ structure (phase C) with 8 H₂O pfu [$a = 13.9014(12)$, $b = 8.9469(8)$, $c = 13.9697(14)$ Å, $V = 1737.5(3)$ Å³] occurred. This phase C has strongly compressed elliptical channels with Ca ions bonding to adjacent walls. At high temperature (300 °C), the quality of the diffraction pattern in path I further degraded and became inclusive.

In path II the diffraction patterns were of considerably higher quality and at 75 °C the phase LT $I2/a$ with 16 H₂O pfu [$a = 9.790(2)$, $b = 10.437(2)$, $c = 9.790(2)$ Å, $\beta = 90.97(3)^\circ$, $V = 1000.1(4)$ Å³] formed, changing at 150 °C to HT $I2/a$ [at 225 °C: $a = 9.434(4)$, $b = 9.044(2)$, $c = 9.695(2)$, $\beta = 89.04(1)^\circ$, $V = 827.0(4)$ Å³] with 4 H₂O. Above 250 °C the HT $I2/a$ structure topotactically transformed by a reconstructive mechanism to a triclinic $C\bar{1}$ Ca feldspar structure [$a = 8.152(5)$, $b = 12.917(5)$, $c = 7.126(4)$ Å, $\alpha = 93.26(3)$, $\beta = 116.37(6)$, $\gamma = 88.72(5)^\circ$, $V = 671.2(7)$ Å³], which does not follow Loewenstein's (1954) rule, as the framework has ordered corner-linked AlO_4 tetrahedra. As a consequence of the **GIS** to Ca feldspar transformation T-O bonds within four-membered rings break and reconnect to a new framework type. The HT $I2/a$ structure with strongly twisted double crankshaft chains acts as precursor for the feldspar formation without an intermediate X-ray amorphous phase usually found after complete dehydration of most natural zeolites.

This study reports for the first time a low-temperature topotactic transformation from gismondine to Ca feldspar and explains the highly unusual occurrence of ordered Al-O-Al clusters in this feldspar structure.

Keywords: Zeolite, gismondine, dehydration, crystal structure, Ca feldspar, Loewenstein's rule

INTRODUCTION

There are four natural zeolite species with corresponding tetrahedral framework topology (framework type **GIS**): gismondine $\text{Ca}_4(\text{Al}_8\text{Si}_8\text{O}_{32})\cdot 18\text{H}_2\text{O}$, garronite $\text{Ca}_{2.5}\text{Na}(\text{Al}_6\text{Si}_{10}\text{O}_{32})\cdot 14\text{H}_2\text{O}$, gobbinsite $\text{Na}_4\text{Ca}(\text{Al}_6\text{Si}_{10}\text{O}_{32})\cdot 12\text{H}_2\text{O}$, and amicitite $\text{Na}_4\text{K}_4(\text{Al}_8\text{Si}_8\text{O}_{32})\cdot 10\text{H}_2\text{O}$ (Coombs et al. 1997; Armbruster and Gunter 2001). The topology of the **GIS** framework is tetragonal, space group $I4_1/amd$. The lowering of the symmetry in minerals with **GIS** framework is due to Si,Al order and ordered incorporation of channel occupants.

The structure of gismondine at room temperature is monoclinic space group $P2_1/c$ with $a \approx 10.02$, $b \approx 10.61$, $c \approx 9.84$ Å, $\beta \approx 92.4^\circ$. In this setting **a** and **c** correspond to the **a** axes of the tetragonal **GIS** framework. Alternating SiO_4 and AlO_4 tetrahedra build four-membered rings connected to double-crankshafts that

run parallel to the **a** and **c** axes. These are linked so that eight-membered channels run parallel to these axes as well. Large, ovoid cavities are formed at the intersection of the channels. These cavities are occupied by extraframework Ca ions bonded to two framework O along one side of the cavity, and four H₂O molecules on the opposite side. In general, one H₂O site is split, resulting in variable Ca coordination. Gismondine has the same Ca:Al:Si ratio of 1:2:2 as anorthite.

Before the gismondine structure had been solved, Smith and Rinaldi (1962), with later revisions by Smith (1968), classified framework structures formed by four- and eightfold rings. They distinguished two ways how chains built by four-membered rings of UDD type can be crosslinked. The UDD nomenclature (Smith and Rinaldi 1962) indicates that within the four-membered rings two adjacent tetrahedra point upward (U) and the other two downward (D). The two different connections lead either (1) to a *flexible* framework or (2) to an *inflexible* framework

* E-mail: thomas.armbruster@krist.unibe.ch

(Smith 1968). As both frameworks of tetrahedra (T) are results of different connectivity, they cannot be transformed into each other without breaking T-O-T connections. The framework of gismondine belongs to the *flexible* type, whereas the framework of feldspar is of the *inflexible* type.

Detailed structural analysis of fully hydrated gismondine was first carried out by Fischer (1963), and was later confirmed by Rinaldi and Vezzalini (1985) who refined the structures of two additional samples and located the H sites for fully occupied H₂O positions. Artioli et al. (1986) applied neutron single-crystal diffraction to explore H₂O disorder in the cavities of the gismondine structure at 15 K and determined the complete system of hydrogen bonds.

Experimentalists later attempted to characterize gismondine in various states of dehydration. Van Reeuwijk (1971) used differential thermal analysis (DTA) combined with thermogravimetry (TG) to evaluate the degree of hydration of the various partly dehydrated phases, which were identified by temperature dependent (up to 450 °C) continuous X-ray photographs using the Guinier method. While heating gismondine, van Reeuwijk (1971) found that five metastable phases were created, at ca. 70, 87, 108, 196, and 280 °C before a Ca feldspar structure formed at 350 °C. The formation of feldspar at such a low temperature without an intermediate X-ray amorphous phase was observed in several other members of the phillipsite group [probably a group combining phillipsite and gismondine defined by Meier (1968)] and deviates from what is exhibited by most other zeolites. Apparently the structure of the preceding phase is sufficiently favorable for such a direct transformation.

Structural studies of partly dehydrated gismondine have been first limited to crystals treated in capillaries under vacuum with subsequent single-crystal X-ray data collection (Vezzalini et al. 1993). Crystals heated up to 290 °C by the same authors displayed an X-ray diffraction pattern with strongly smeared reflections precluding determination of cell dimensions and symmetry. Gismondine treated 1 h under vacuum lost ca. 10% H₂O. Rearrangement of H₂O led to space group $P2_1$ with little influence on the tetrahedral framework. The diffraction pattern of gismondine treated 24 h under vacuum corresponded to the one obtained by heating the crystal to 80 °C. This gismondine lost ca. 50% H₂O and had a doubled unit-cell volume with the orthorhombic space group $P2_12_12_1$. The corresponding structure is distorted leading to strongly squashed channel systems.

Temperature induced dehydration with simultaneous collection of synchrotron powder X-ray diffraction data was done by Milazzo et al. (1998). In close agreement with van Reeuwijk (1971) four partially dehydrated gismondine phases were found. Phase B analyzed between 80 and 100 °C and phase C between 100 and 205 °C have both space group $P2_12_12_1$ and the same composition Ca₄(Al₈Si₈O₃₂)·8H₂O, though different unit-cell volume 1995.2 (phase B) vs. 1797.8 Å³ (phase C). Phase C corresponds to the one analyzed by Vezzalini et al. (1993) after 24 h vacuum treatment. Phase D found between 205 and 440 °C could not be structurally characterized.

The purpose of this study is to unravel the structural complexity of gismondine upon dehydration using single-crystal XRD (X-ray diffraction) conjoined with step-wise heating to elevated temperatures. In particular, the question will be addressed why

dehydrated gismondine transforms directly to an anorthite-like structure, whereas most other natural zeolite form an intermediate X-ray amorphous product. This study uses the same experimental approach as successfully applied to the zeolites goosecreekite (Wadoski et al. 2011) and parthéite (Lazic et al. 2012) and the zeolite-like structures of cavansite (Danisi et al. 2012) and pentagonite (Danisi et al. 2013). All these studies were performed to define general rules how zeolites behave with increasing temperature upon dehydration (Cruciani 2006).

EXPERIMENTAL METHODS

The studied gismondine originated from Rio Pian del Foco, Olbicella, Genova province, Italy (Cortesogno et al. 1975). The crystals with pseudo-octahedral forms separated from the surface of strongly transformed metagabbro are up to 3 mm in dimension and are generally twinned (Cortesogno et al. 1975).

Five single crystals were removed from the sample and mounted in acrylic resin and subsequently ground and polished for electron microprobe analysis. Samples were compositionally analyzed on a JEOL JXA8200 electron microprobe for Al (anorthite), Si (orthoclase), Cl (scapolite), Na (albite), K (orthoclase), Mg (forsterite), Ca (anorthite), F (phlogopite), Fe (almandine), and Cr (eskolait). Operating conditions for six analyses on each of the five crystals were 15 kV accelerating voltage, 20 nA beam current, and a 30 μm spot size.

SINGLE-CRYSTAL XRD

Several crystals were broken in an agate mortar to dimensions below 0.2 mm and examined under crossed polarizers to select untwinned single crystals. The chosen crystal fragments were placed in open 0.2 mm diameter quartz glass capillaries and heated in 25 °C increments to 225 °C under a constant dry nitrogen stream using an Oxford Cryostream Plus 700 Series. The samples were held for 1 h before data collection. Single-crystal XRD was carried out on a Bruker APEX II diffractometer with MoK α (0.71073 Å) X-ray radiation with 50 kV and 40 mA X-ray power. Above 225 °C, an in-house designed regulated nitrogen stream-heater attachment was used. Samples were heated in 25 °C steps to 400 °C, held at temperature for 1 h and measured. From 425 to 600 °C (in 25 °C steps) the procedure was the same, but only the lattice parameters were determined. Experiments were conducted on ~10 crystal fragments for various reasons. (1) Some crystals fractured during the heating excursion or contracted in volume thus their position and fixation became unstable in the capillary. (2) The heating experiments led to diverging diffraction patterns thus the experiments were repeated on additional crystals for better understanding. CCD data were integrated and empirically absorption-corrected using the Apex2 v. 2009–11.0 software package (Bruker 2009). The structures were refined with SHELXL Version 2008/4 or Beta test 2013/1 (Sheldrick 2008) using neutral atom scattering factors. At room temperature the structure was refined including the H positions of the fully occupied H₂O sites using the restraints $d(O-H) = 0.95(1)$ Å and $d(H-H) = 1.59(5)$ Å. The Ca position was split into two closely spaced subsites. Ignoring the influence of minor extraframework Na, the sum of occupancies at the subsites Ca1 and Ca2 was fixed at 1 Ca. The nomenclature of atomic coordinates for the $P2_1/c$ RT data set was adopted from Artioli et al. (1986). Starting coordinates of the HT $P2_12_12_1$ structure were taken from Vezzalini et al. (1993). At elevated temperature the sum of Ca occupancies remained unconstrained in **GIS** type frameworks but was constrained to 1 for the Ca feldspar structure based on poor diffraction data. The reason for the unconstrained Ca occupancies for good diffraction data at elevated temperature is possible Ca disorder. If the refined Ca occupancies converged to a value below the stoichiometric composition, dispersed disorder or overlay with H₂O sites must be assumed. The triclinic $C\bar{1}$ feldspar structure was highly twinned and the strongly broadened reflections were integrated for the two major twin contributors related by 180° rotation about the reciprocal axis (−0.50, 1.0, 0.474). A summary of structures refined along path 1 is given in Table 1 and experimental details for structures according to path II are summarized in Table 2.

RESULTS

The polished surface of the samples used for electron microprobe analyses in carbon-coated thin sections deteriorated noticeably under vacuum alone. The composition was stoichiometrically consistent with the ideal chemical formula with minor amounts of F and Na [0.035 and 0.035 apfu (normalized to 1 Ca

TABLE 1. Parameters for X-ray data collection with APEX II SMART using graphite monochromated MoK α X-radiation, $\lambda = 0.71073$ Å, and parameters of crystal-structure refinements of gismondine Ca₄(Al₆Si₈O₃₂)·18H₂O upon dehydration according to path I

Crystal data	Gismondine RT Phase A	Gismondine LT P2 ₁ 2 ₁ Phase B	Gismondine HT P2 ₁ 2 ₁ Phase C
Temperature (°C)	25	75	150
Unit cell (Å)	$a = 10.0214(1)$ $b = 10.5997(1)$ $c = 9.8327(1)$ $\beta = 92.363(1)^\circ$	$a = 13.6801(8)$ $b = 10.4670(6)$ $c = 13.8667(9)$ Orthorho.	$a = 13.9014(12)$ $b = 8.9469(8)$ $c = 13.9697(14)$ Orthorho.
Volume (Å ³)	1043.58(2)	1985.6(2)	1737.5(3)
Space group	P2 ₁ /c (No. 14)	P2 ₁ 2 ₁ 2 ₁ (No. 19)	P2 ₁ 2 ₁ 2 ₁ (No. 19)
Z	1	2	2
H ₂ O pfu per Ca ₄	18	12	8
Intensity measurement			
Max. θ°	37.40	35.07	27.62
Index ranges	$-17 \leq h \leq 9$ $-17 \leq k \leq 17$ $-15 \leq l \leq 16$	$-21 \leq h \leq 21$ $-16 \leq k \leq 16$ $-22 \leq l \leq 21$	$-17 \leq h \leq 18$ $-11 \leq k \leq 11$ $-18 \leq l \leq 16$
No. meas. refl.	19877	44770	25879
No. unique. refl.	4910	8142	4011
No. obs. refl. [$I > 2\sigma(I)$]	3981	6784	2765
Refinement of the structure			
No. of variables	204 + 9 restraints	289	277
R_{int}	0.0323	0.0745	0.1169
R_σ	0.0353	0.0617	0.0769
$R1, I > 2\sigma(I)$	0.0341	0.0624	0.1188
$R1, all data$	0.0442	0.1204	0.1586
$wR2 (on F^2)$	0.1041	0.3132	0.3921
Goof	1.058	1.309	1.486
$\Delta\rho_{min} (-e/\text{Å}^3)$	-0.91 near Ca2	-2.20 near W4	-1.43 near Si1
$\Delta\rho_{max} (e/\text{Å}^3)$	0.65 near O6	6 near Si4) ^a	2.25 near O14

^a Several ghost peaks of ca. 6 (e/Å³) appeared in the final difference-Fourier map. These peaks are related to an additional phase appearing coherently intergrown with phase B (LT P2₁2₁2₁). Refinement of the ghost peaks with Si scattering factors led to occupancies of ca. 17%.

pfu), respectively]. In particular, there was no significant difference in the composition of several crystals analyzed from the same hand specimen from which the crystals for the dehydration study were also picked. These results were in agreement with those of Cortesogno et al. (1975) reporting close to end-member composition with minor Na.

Below 75 °C the space group of gismondine remains consistent with the one at room temperature, with only 0.17% reduction of volume from 25 to 50 °C due to decrease of H₂O from 18 to 17.2 pfu. Multiple heating measurements were conducted with surprising results. Differing from previously published studies (Milazzo et al. 1998), we found that at ca. 75 °C, the structure of the gismondine crystals would diverge along two paths; either to space group P2₁2₁2₁ associated with a very poor, smeared diffraction pattern or to an I2 (or I2/a depending on data set) structure with a rather sharp diffraction pattern. Structures with space groups I2 or I2/a were characterized by a well-defined I-centered lattice with few significant but weak reflections violating a glide. However, refinements in space group I2 yielded structure models, which were essentially of I2/a symmetry but with twice as many variables as corresponding refinements in space group I2/a. In addition, the I2 refinements were not superior to the I2/a refinements. Thus the latter models are reported (Tables 2 and 3). Above 150 °C a non-standard I2/a setting with $\beta < 90^\circ$ was used to maintain the same axial orientation as for the refinements at lower temperature. Structural data for the HT

TABLE 2. Parameters for X-ray data collection with APEX II SMART using graphite monochromated MoK α X-radiation, $\lambda = 0.71073$ Å, and parameters of crystal-structure refinements of gismondine Ca₄(Al₆Si₈O₃₂)·18H₂O upon dehydration according to path II and its dehydrated variety [Ca feldspar: Ca(Al₂Si₂O₈)]

Crystal data	Gismondine LT I2/a	Gismondine HT I2/a	Ca feldspar
Temperature (°C)	75	225	350
Unit cell (Å)	$a = 9.790(2)$ $b = 10.437(2)$ $c = 9.790(2)$ $\beta = 90.97(3)^\circ$	$a = 9.434(4)$ $b = 9.044(2)$ $c = 9.695(2)$ $\beta = 89.04(1)^\circ$	$a = 8.152(5)$ $b = 12.917(5)$ $c = 7.126(4)$ $\alpha = 93.26(3)^\circ$ $\beta = 116.37(6)^\circ$ $\gamma = 88.72(5)^\circ$
Volume (Å ³)	1000.1(4)	827.0(4)	671.2(7)
Space group	I2/a (No. 15)	I2/a (No. 15)	C $\bar{1}$ (No. 2)
Z	1	1	4
H ₂ O pfu	16	4	0
Intensity measurement			
Max. θ°	36.60	39.8	33.01
Index ranges	$-16 \leq h \leq 16$ $-16 \leq k \leq 17$ $-16 \leq l \leq 15$	$-16 \leq h \leq 12$ $-15 \leq k \leq 13$ $-17 \leq l \leq 17$	$-12 \leq h \leq 9$ $-18 \leq k \leq 10$ $-10 \leq l \leq 10$
No. meas. refl.	6801	10729	1355
No. unique. refl.	1650	2403	1353
No. obs. refl. [$I > 2\sigma(I)$]	1284	1723	946
Refinement of the structure			
No. of variables	120	80	118
R_{int}	0.0466	0.0435	0.0979
R_σ	0.0470	0.0408	0.0967
$R1, I > 2\sigma(I)$	0.0628	0.0474	0.1022
$R1, all data$	0.0786	0.0721	0.1404
$wR2 (on F^2)$	0.1825	0.1239	0.2966
Goof	1.497	1.098	1.139
$\Delta\rho_{min} (-e/\text{Å}^3)$	-0.55 near Al	-0.58 near Si	-1.2 near O _{8m}
$\Delta\rho_{max} (e/\text{Å}^3)$	0.76 near OW1	0.71 near Ca1	1.2 near O _{2m}

I2/a structure are given for data collected at 225 °C (Tables 2 and 3) because refinement results were of higher quality than those obtained at lower temperature. Five additional heating trials were attempted to determine if the rate of heating played a role in determining which “path” the crystal would take. Three samples were heated slowly (approximately 4 °C/min) and lattice dimensions measured. Two samples were raised to 75 °C rapidly (approximately 30 °C/min) and lattice dimensions measured. The results were inconclusive. All 5 samples transformed to the P2₁2₁2₁ space group at 75 °C (path I), and not to I2/a (path II). In accordance with Vezzalini et al. (1993) the orthorhombic P2₁2₁2₁ setting with doubled volume may be obtained from the original P2₁/c setting by the matrix [101/010/-101]. The quality of the high-temperature (300 °C) diffraction patterns of the crystals following path I further degraded and were inclusive. Above 250 °C the I2/a structures (path II) transformed to a triclinic feldspar structure of space group C $\bar{1}$ with strongly smeared diffraction patterns. Table 3 displays atomic coordinates, isotropic displacement parameters, and occupancies of natural gismondine and all dehydrated phases found in path II. Table 4¹ (deposited) contains all CIF files¹ of refined structures showing also anisotropic displacement parameters and bond lengths.

¹ Deposit item AM-13-1101, Table 4 and CIFs. Deposit items are available two ways: For a paper copy contact the Business Office of the Mineralogical Society of America (see inside front cover of recent issue) for price information. For an electronic copy visit the MSA web site at <http://www.minsocam.org>, go to the *American Mineralogist* Contents, find the table of contents for the specific volume/issue wanted, and then click on the deposit link there.

TABLE 3a. Atomic coordinates, U_{eq} , and occupancies of gismondine at room temperature, space group $P2_1/c$ with $18H_2O$ pfu [$a = 10.0214(1)$, $b = 10.5997(1)$, $c = 9.8327(1)$ Å, $\beta = 92.363(1)^\circ$, $V = 1043.58(2)$ Å³]

Site	Atom	x	y	z	U_{eq}/U_{iso}	Occ.
Si1	Si	0.41466(3)	0.11265(3)	0.18172(3)	0.00791(7)	1
Si2	Si	0.90803(3)	0.86989(3)	0.16043(3)	0.00807(7)	1
Al1	Al	0.09669(4)	0.11315(3)	0.16898(4)	0.00806(8)	1
Al2	Al	0.59069(4)	0.86664(3)	0.14869(4)	0.00840(8)	1
Ca1	Ca	0.71584(11)	0.07706(5)	0.35506(5)	0.03260(17)	0.898(3)
Ca2	Ca	0.7656(9)	0.0735(6)	0.3411(5)	0.03260(17)	0.102(3)
O1	O	0.07975(12)	0.15644(11)	0.00011(10)	0.0199(2)	1
O2	O	0.26200(10)	0.07645(10)	0.21320(11)	0.01744(19)	1
O3	O	0.43436(11)	0.14800(10)	0.02494(9)	0.01679(19)	1
O4	O	0.24443(10)	0.40355(11)	0.30367(11)	0.01680(19)	1
O5	O	0.00001(12)	0.98590(10)	0.21336(11)	0.0212(2)	1
O6	O	0.04550(10)	0.24264(9)	0.26038(10)	0.01675(18)	1
O7	O	0.46405(11)	0.22850(9)	0.27766(9)	0.01574(18)	1
O8	O	0.51116(10)	0.99406(9)	0.22607(9)	0.01262(16)	1
OW1	O	0.25920(16)	0.10418(15)	0.50260(13)	0.0340(3)	1
OW2	O	0.59255(15)	0.12702(13)	0.54227(15)	0.0316(3)	1
OW3	O	0.91067(16)	0.11644(14)	0.50028(15)	0.0356(3)	1
OW4	O	0.7720(4)	0.2377(4)	0.2350(5)	0.0553(14)	0.508(5)
OW5	O	0.7417(4)	0.3172(3)	0.4044(5)	0.0570(14)	0.492(5)
OW6A	O	0.7788(10)	0.2036(10)	0.1636(11)	0.0450(18)	0.25
OW6B	O	0.7517(9)	0.1657(9)	0.1153(9)	0.0450(18)	0.25
H11	H	0.222(4)	0.1861(19)	0.514(4)	0.096(14)*	1
H21	H	0.258(4)	0.102(4)	0.4053(10)	0.094(13)*	1
H12	H	0.545(3)	0.2042(17)	0.534(3)	0.058(9)*	1
H22	H	0.556(4)	0.078(3)	0.612(3)	0.101(14)*	1
H13	H	0.951(3)	0.1977(16)	0.496(3)	0.068(10)*	1
H23	H	0.926(3)	0.070(3)	0.580(2)	0.073(10)*	1

Note: Values in the corresponding column determined with U_{iso} are marked by an asterisk.

TABLE 3b. Atomic coordinates, U_{eq} , and occupancies of gismondine at 75 °C space group $I2/a$ with 16 H_2O pfu [$a = 9.790(2)$, $b = 10.437(2)$, $c = 9.790(2)$ Å, $\beta = 90.97(3)^\circ$, $V = 1000.1(4)$ Å³]

Site	Atom	x	y	z	U_{eq}/U_{iso}	Occ.
Si	Si	0.06981(7)	0.35773(7)	0.34690(9)	0.0134(2)	1
Al	Al	0.10332(8)	0.11131(8)	0.16930(10)	0.0140(2)	1
Ca1	Ca	0.3047(5)	-0.0854(4)	0.3313(5)	0.0362(17)	0.254(13)*
Ca2	Ca	-0.0947(4)	0.1612(4)	0.5544(6)	0.0361(16)	0.186(5)*
O1	O	-0.0369(3)	0.4629(2)	0.2857(3)	0.0277(5)	1
O2	O	0.0528(3)	0.3419(3)	0.5079(3)	0.0302(5)	1
O3	O	0.0310(2)	0.2210(2)	0.2800(3)	0.0267(5)	1
O4	O	0.2784(2)	0.0968(3)	0.1954(4)	0.0307(7)	1
OW1	O	0.2261(12)	-0.2820(15)	0.4124(17)	0.076(6)	0.395(19)
OW2	O	-0.0298(13)	0.0590(18)	0.5103(17)	0.129(8)	0.60(3)
OW3	O	-0.1621(17)	-0.0303(19)	0.4980(18)	0.099(8)	0.41(2)
OW4	O	0.276(2)	-0.149(6)	0.296(4)	0.17(2)	0.51(5)
OW5	O	0.245(2)	-0.239(3)	0.309(3)	0.032(8)*	0.13(3)

*The sum of Ca occupancies yielding 3.5 Ca pfu is different to the stoichiometric value of 4.0 Ca pfu due to unresolved Ca disorder and/or overlay with OW sites.

DISCUSSION

The room-temperature results of Rio Pian del Foco gismondine are in agreement with previous studies by Rinaldi and Vezzalini (1985). The two types of possible H_2O configurations are also confirmed. Either OW4 is occupied or OW5 together with OW6A or OW6B. The same $P2_1/c$ GIS framework structure determined at room temperature (Table 1) remained stable up to 50 °C before the dehydration pathways diverged depending on the selected crystal fragment. The preference of one of the dehydrations routes depending on chemical variations is highly unlikely and not supported by our electron microprobe analyses, yielding consistent composition. We speculate that the choice of dehydration path may depend on the orientation of the crystal relative to the confining capillary walls. As the crystals were squeezed into the capillary, orientation-dependent stress or strain has to be expected.

TABLE 3c. Atomic coordinates, U_{eq} , and occupancies of gismondine at 225 °C space group $I2/a$ with $4H_2O$ pfu [$a = 9.434(4)$, $b = 9.044(2)$, $c = 9.695(2)$, $\beta = 89.04(1)^\circ$, $V = 827.0(4)$ Å³]

Site	Atom	x	y	z	U_{eq}/U_{iso}	Occ.
Si	Si	0.05556(6)	0.32064(6)	0.38602(5)	0.01788(12)	1
Al	Al	0.13201(6)	0.07978(7)	0.18112(6)	0.01776(13)	1
Ca1	Ca	-0.17893(13)	0.20622(15)	0.18672(19)	0.0383(5)	0.389(3)*
Ca2	Ca	0.0640(8)	0.0484(6)	0.5680(6)	0.0318(18)	0.084(3)*
O1	O	-0.09122(16)	0.39158(17)	0.32814(17)	0.0246(3)	1
O2	O	0.0500(2)	0.3228(2)	0.55227(16)	0.0330(4)	1
O3	O	0.0627(2)	0.15111(18)	0.33389(17)	0.0297(3)	1
O4	O	0.18636(19)	0.4183(2)	0.3271(2)	0.0379(4)	1
OW1	O	0.25	-0.1164(8)	0.5	0.124(2)	1

*The sum of Ca occupancies yielding 3.8 Ca pfu is different to the stoichiometric value of 4.0 Ca pfu due to unresolved Ca disorder and/or overlay with the OW site.

TABLE 3d. Atomic coordinates, U_{eq} , and occupancies of Ca feldspar 350 °C, space group $C1$ [$a = 8.152(5)$, $b = 12.917(5)$, $c = 7.126(4)$ Å, $\alpha = 93.26(3)^\circ$, $\beta = 116.37(6)^\circ$, $\gamma = 88.72(5)^\circ$, $V = 671.2(7)$ Å³]

Site	Atom	x	y	z	U_{eq}/U_{iso}	Occ.
T ₁ O	Al	-0.5099(5)	0.1673(4)	-0.2113(6)	0.0185(10)	1
T ₁ m	Si	0.0040(5)	0.3201(3)	-0.2343(6)	0.0166(9)	1
T ₂ O	Al	-0.1872(5)	0.1137(4)	-0.3146(6)	0.0174(10)	1
T ₂ m	Si	-0.1790(5)	-0.1172(3)	-0.3603(6)	0.0157(9)	1
Ca1	Ca	0.2356(7)	-0.0197(7)	-0.1592(10)	0.0429(18)	0.729(14)
Ca2	Ca	0.223(2)	0.0208(19)	-0.096(3)	0.0429(18)	0.271(14)
O ₁	O	-0.5206(15)	0.1296(11)	0.0245(16)	0.033(3)	1
O ₂	O	-0.0791(13)	-0.0074(10)	-0.2830(17)	0.026(3)	1
O ₃ O	O	-0.3101(14)	0.1110(10)	-0.1739(17)	0.032(3)	1
O ₃ m	O	0.1825(15)	0.3567(11)	-0.260(2)	0.037(3)	1
O ₄ O	O	-0.0215(14)	-0.2039(10)	-0.2780(19)	0.030(3)	1
O ₄ m	O	-0.0030(15)	0.1935(11)	-0.2124(19)	0.033(3)*	1
O ₅ O	O	-0.7077(14)	0.1075(10)	-0.3863(17)	0.028(3)	1
O ₅ m	O	-0.3198(16)	0.1289(11)	-0.5826(18)	0.036(3)	1

Path I

The most common path I, also observed by Milazzo et al. (1998), yielded at 75 °C the B-type structure named here LT $P2_12_12_1$ (Table 1 and Fig. 1). The orthorhombic phase has a doubled volume relative to the monoclinic room-temperature structure. Normalized to the volume at 50 °C, the LT $P2_12_12_1$ structure shows a volume reduction of only 4.7%. At 150 °C the crystal preserved symmetry (named HT $P2_12_12_1$) but the cell volume decreased 16.7% normalized to the monoclinic $P2_1/c$ structure at 50 °C. Based on the complexity of the observed diffraction pattern we assume that in the intermediate temperature range both $P2_12_12_1$ structures coexist. Milazzo et al. (1998) named the two phases B and C, both of identical composition $Ca_4(Al_8Si_8O_{32}) \cdot 8H_2O$. This is not confirmed by our study. For LT $P2_12_12_1$ we located 12 H_2O pfu and for HT $P2_12_12_1$ 8 H_2O pfu. The different H_2O content is also supported by the strong difference in unit-cell volume, 1985.6(2) Å³ (LT $P2_12_12_1$) vs. 1737.5(3) Å³ (HT $P2_12_12_1$). Ca1 and Ca2 in LT $P2_12_12_1$ are both eight-coordinated by four framework O and four H_2O . HT $P2_12_12_1$ (Fig. 1) has strongly compressed elliptical channels running parallel to [101] and [10 $\bar{1}$] with Ca ions bonding to adjacent walls of the channels. Three bonds to H_2O molecules and four bonds to framework O complete the sevenfold Ca coordination. The channels of LT $P2_12_12_1$ have less elliptical cross sections and Ca only bonds to one flank of the channel wall. An additional orthorhombic phase is reported between 205 and 440 °C (Milazzo et al. 1998), but this structure was not explored by us because of poor diffraction behavior. The temperature dependence of the unit-cell volume according to path I is shown in Figure 2.

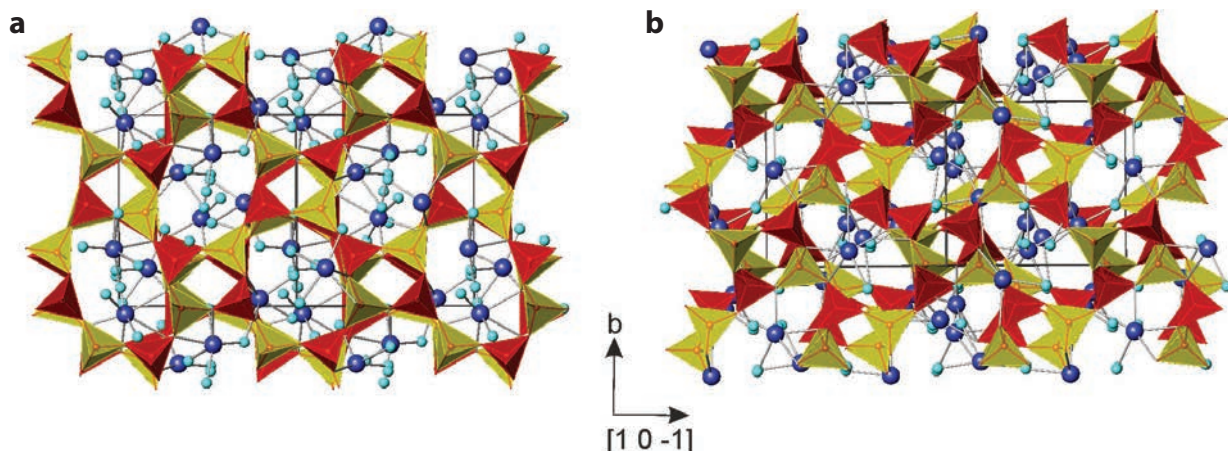


FIGURE 1. Tetrahedral frameworks analyzed for gismondine dehydration along path I. AlO_4 tetrahedra are yellow and SiO_4 tetrahedra are red. Ca spheres are dark blue, H_2O molecules are light blue. (a) LT $P2_12_12_1$ structure with 12 H_2O at 75 °C, named phase B by Milazzo et al. (1998); (b) HT $P2_12_12_1$ structure with 8 H_2O forming at 150 °C, named phase C by Milazzo et al. (1998). The structural drawing represents the structure at 225 °C. The eight-membered rings are strongly squashed and Ca bonds to opposite channel walls (Vezzalini et al. 1993).

Path II

For the less frequent, newly detected path II we analyzed at 75 °C a structure with strongly disordered Ca and H_2O sites (Fig. 3) of space group $I2/a$ named here LT $I2/a$ (Table 2). With rising temperature, the complex diffraction pattern indicated that the latter structure coexists with a new $I2/a$ structure (Fig. 3), which becomes dominant at 150 °C, named HT $I2/a$. The unit-cell volume of the HT $I2/a$ structure (Table 2) decreased 21% relative to the $P2_1/c$ structure at 50 °C. This contraction is associated with loss of ca. 14 H_2O pfu. Thus, a Ca/ H_2O ratio of 1/1 results. Ca is split over two major sites, each coordinated by five framework oxygen atoms and one H_2O molecule (Fig. 3).

Above 250 °C the HT $I2/a$ structure transforms to a triclinic $C\bar{1}$ anhydrous feldspar-related structure (Table 2), which does not follow Loewenstein's (1954) rule, as the new framework shows corner-linked AlO_4 tetrahedra. This indicates that for the topotactic transformation of the gismondine $I2/a$ structure to the anhydrous feldspar structure T-O-T bonds were broken. The topotactic type of the transformation is indicated by the existence of a twinned single-crystal diffraction pattern of the Ca feldspar. The temperature dependence of the unit-cell volume according to path II is shown in Figure 2.

Structural differences of GIS frameworks in path I and II

The major difference of partly dehydrated gismondine structures in path I and path II is the arrangement of the eight-membered rings of tetrahedra perpendicular to the channel axes. Structures in path I have strongly elliptically deformed eight-membered rings (Fig. 1). Along the channel axes adjacent eight-membered rings have the longest and shortest half axes of the elliptical cross section parallel to each other. Structures in path II show also strongly elliptically deformed eight-membered rings. However, along the channel axes the adjacent eight-membered rings are rotated 90° against each other, thus the shortest half axis of the elliptical cross section is aligned with the longest one above and below (Fig. 3). As a consequence, if the structures

are viewed along the channel axes, the open space has almost quadratic cross section. It seems that the energetic difference between the two possibilities of ring stacking is very low and minor effects such as strain or stress are responsible whether path I or II is preferred.

The high-temperature $I2/a$ structure as precursor of a novel Ca feldspar

The special feature of the HT $I2/a$ gismondine structure is the opposing sense of rotation of the four-membered rings along the **a** and **c** axes (Figs. 3 and 4). At room temperature these rings appear overlain and at above 75 °C the opposing rotation begins, though at first in a moderate way. While this type of $I2/a$ dehydration structure was hitherto unknown for gismondine, a very similar structure has been reported for dehydration (6 days at 6×10^{-7} bar) of amicitite $\text{Na}_4\text{K}_4(\text{Al}_8\text{Si}_8\text{O}_{32}) \cdot 10\text{H}_2\text{O}$ (Vezzalini et al. 1999) with space group $I2$. Amicite of GIS framework type has the same framework stoichiometry as gismondine but different ionic channel occupants (Na, K). Another related but less pronounced deformation of the GIS framework has been determined for Rb ion-exchanged gismondine (Bauer and Baur 1998).

The opposing rotation sense of the four-membered rings within the double crankshaft chains imposes a severe strain on the rings (Fig. 4). Within these chains, planar four-membered rings alternate with strongly twisted rings (Fig. 5). As summarized by Alberti and Martucci (2011) such twisted four-membered rings are preferred locations for T-O-T rupture leading to reconstructive phase transformations. This is what happens with increasing temperature when the $I2/a$ gismondine structure further dehydrates and transforms to a Ca feldspar structure. After the twisted rings break (Fig. 5), the affected tetrahedra reconnect to the closest T sites in the adjacent four-ring, building a new type of double crankshaft chain. The newly formed T-O-T connections occur between tetrahedral sites centered by the same cation type (Fig. 5). Thus, in addition to Si-O-Si links, Al-O-Al units are also created, which contradicts Loewenstein's

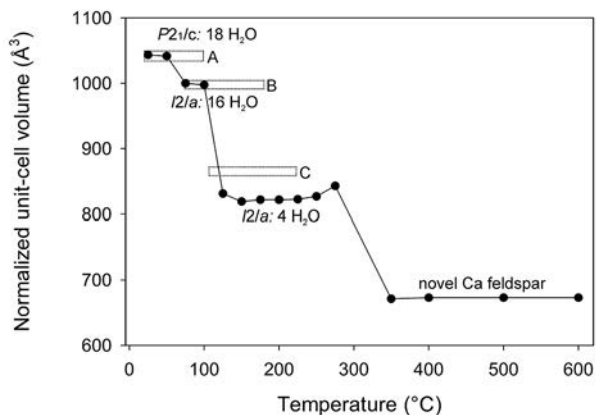


FIGURE 2. Temperature dependence of normalized unit-cell volume for gismondine upon dehydration. From room temperature to formation of the novel Ca feldspar the volume decreases by 26%. Black dots symbolize measurements following dehydration path II (this study). The symbol size is considerably larger than e.s.d. values of corresponding measurements. Boxes with dotted outlines labeled A, B, and C represent temperature dependence of gismondine volume for dehydration following path I (Milazzo et al. 1998).

(1954) rule. In other words, the feldspar structure forming upon complete dehydration of gismondine is different to anorthite, which shows in the ideal case a strict alternation of Si and Al filled tetrahedra. Nevertheless, the tetrahedral topology of the feldspar topotactically derived from gismondine is the same as the one of anorthite.

Another problem remains to be explained: In a **GIS** framework there are two sets of double-crankshaft chains running parallel to **a** and **c**, whereas in feldspar such chains only occur in one direction. In the **GIS** framework, the two perpendicularly oriented double-crankshaft chains are not independent. In the *I2/a* structure obtained by dehydration, both chains have the twisted four-rings in common. Rupture of this twisted ring and formation of a new T-O-T connection pattern reestablishes one crank-shaft but the second crankshaft originally running perpendicular to the first one no longer exists due to the newly formed links. Loss of this interwoven system of double crankshafts also relaxes the strain inherited from the twisted gismondine framework and the remaining crankshaft in the newly formed feldspar structure may adopt a more compressed arrangement (Fig. 5). In the sense of the studies by Smith and Rinaldi (1962) and Smith (1968), gismondine transforms upon dehydration by a reconstructive process from a *flexible* framework to an *inflexible* one. The existence of only one chain system in feldspar compared to the two chain systems in gismondine explains the observed twinning of Ca feldspar.

The novel Ca feldspar structure and comments on Loewenstein's rule

The new type of Si,Al order observed for the novel Ca-feldspar with Si-O-Si and Al-O-Al sequences along the chain direction [100] of the double crankshafts is inherited by a phase transition from a strongly deformed **GIS** framework (Figs. 4 and 5). The topotactic transformation indicates that the choice of an appropriate precursor-phase (gismondine) enables low-

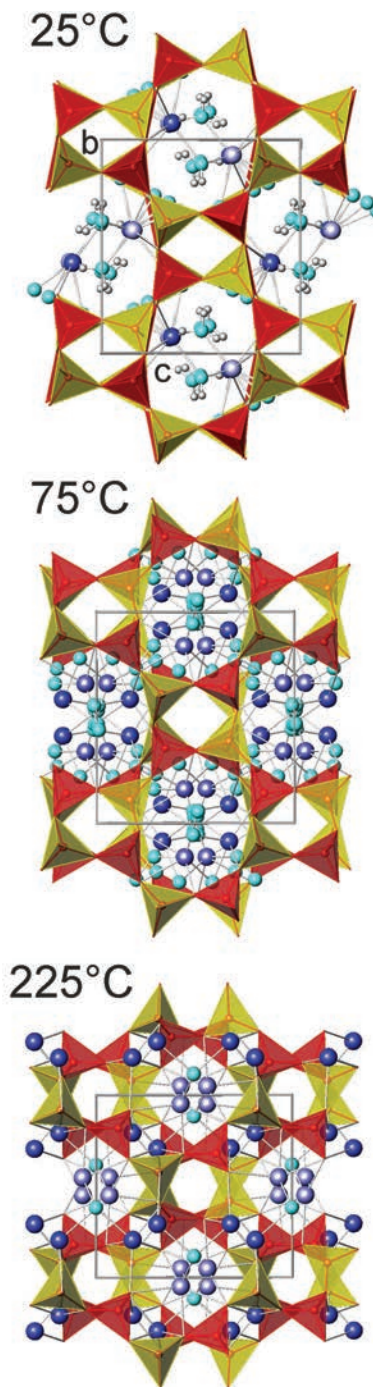


FIGURE 3. Tetrahedral frameworks analyzed for gismondine dehydration along path II. AlO_4 tetrahedra are yellow and SiO_4 tetrahedra are red. Ca spheres are dark blue with intensity shade representing occupancy. H_2O molecules are light blue. The projection along **a** is parallel to double crankshaft chains represented in this view as four-rings. At 25 °C (space group $P2_1/c$) the four-membered rings at different levels along **a** almost perfectly overlap. At 75 °C (space group $LT I2/a$) four-rings at different levels along **a** are slightly rotated in opposite sense. Starting at 150 °C (example shown at 225 °C) the space group is preserved but the $HT I2/a$ structure has four-rings at different level along **a**, which are rotated ca. 30° against each other. The overlay of strongly elliptical eight-ring channels causes almost quadratic apertures parallel to **a**.

temperature synthesis of a new structural variety (feldspar with ordered Al-O-Al), which at first glance would have been considered “highly unlikely” by most crystal chemists. However, one should keep in mind that Loewenstein (1954) drafting the Al-O-Al avoidance rule for tetrahedral Al, perceived this statement just as a rule of thumb. He already stated exceptions and the more minerals and synthetic compounds were structurally studied, the more exceptions of the regular case became evident: e.g., KAlO_2 , space group $Pbca$ (Barth 1935), has a tetrahedral framework structure built by Al tetrahedra only (stuffed cristobalite structure type); there are numerous aluminate sodalities exemplified in the mineral world by bicchulite $\text{Ca}_2[\text{Al}_2\text{SiO}_6](\text{OH})_2$ (Sahl 1980); mayenite $\text{Ca}_{12}\text{Al}_{14}\text{O}_{33}$ (Büsem and Eitel 1936) or its Cl-bearing natural variety (Galuskin et al. 2012) have a cubic tetrahedral framework structure; and gehlenite $\text{Ca}_2[\text{Al}_2\text{SiO}_7]$ has a tetrahedral layer structure (e.g., Kimata and Ii 1984). Quenched from 1530 °C, anorthite with Si/Al ratio of 1 exhibits pronounced Si,Al disorder (Bruno et al. 1976). Thus random Al-O-Al units may exist even in feldspar frameworks.

Unfortunately the novel Ca feldspar structure (Fig. 6) is of low quality, not surprisingly considering the formation conditions and intimate twinning. The structure exhibits strongly anisotropic oxygen atomic displacement parameters indicating librational disorder of tetrahedra with average Si-O and Al-O distances of 1.617 and 1.732 Å, respectively. Ca occupies a split position (Ca1 73% and Ca2 27%) separated by 0.71 Å. Ca1 is six-coordinated with an average Ca1-O distance of 2.522 Å, Ca2 is seven-coordinated with average Ca2-O of 2.604 Å. It remains dubious of whether the Ca splitting is of static or dynamic nature. Monitoring the diffraction pattern of the novel Ca feldspar up to 600 °C confirmed that this phase did not undergo significant structural modifications within the investigated temperature range. The structural stability of this Ca feldspar has two basic principles: (1) Within the $\text{T}_1\text{O}(\text{Al})\text{-O}_B\text{O-T}_2\text{O}(\text{Al})$ units Al-O_BO distances are shortened to 1.69(1) Å. (2) The major Ca site is only six-coordinated, whereas regular anorthite (Bruno et al. 1976) has preferentially seven-coordinated Ca. A low Ca coordination reduces “underbonding” of O_BO. O_BO linking two AlO_4 tetrahedra has an additional bond to the major Ca site (Ca1) of 2.54 Å, whereas O_Bm linking two SiO_4 tetrahedra has an additional bond to the minor Ca site (Ca2) of 2.72 Å. Thus all interatomic distances sensitive of the observed Si,Al order pattern are in agreement with the model. T-O-T angles in the novel Ca feldspar with 4 symmetry-independent T sites vary between 126 and 162°, whereas conventional anorthite with 16 T sites has T-O-T angles between 123 and 170° (Wainwright and Starkey 1971). In spite of the space group $C\bar{1}$ the structure of the novel Ca feldspar is considerably simpler than the one of anorthite (Fig. 6) because the unit-cell volume of the former is only half of that of $P\bar{1}$ anorthite (Wainwright and Starkey 1971).

Could the unusual order pattern of Al-O-Al and Si-O-Si units be an artifact of low data quality and neglect of weak superstructure reflections?

We admit that the data quality of the Ca feldspar is poor. This is not surprising if we consider that T-O-T bonds of the original gismondine were broken and reconnected to new links to accomplish a feldspar structure. Upon gismondine dehydration

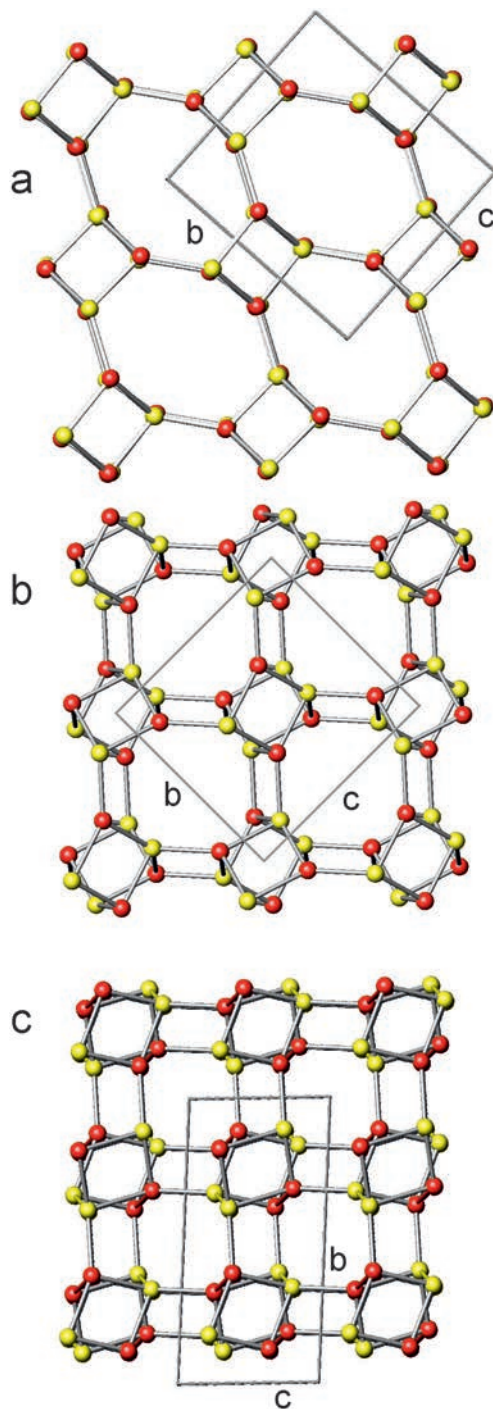


FIGURE 4. Topotactic development of a GIS type framework (a, b) to a Ca feldspar structure (c). For simplicity only the centers of T sites are shown as red Si and yellow Al spheres connected to a framework. Notice the rotation of four-rings. In the case of the $C\bar{1}$ feldspar structure (c), projected along [100], the rotation is so strong that tetrahedra of the same color at different height come so close to each other that they are linked, whereas some former Al-Si links ruptured. (a) Gismondine framework of space group $P2_1/c$ at 25 °C, (b) of space group $I2/a$ at 225 °C, (c) Ca feldspar framework of space group $C\bar{1}$ at 350 °C.

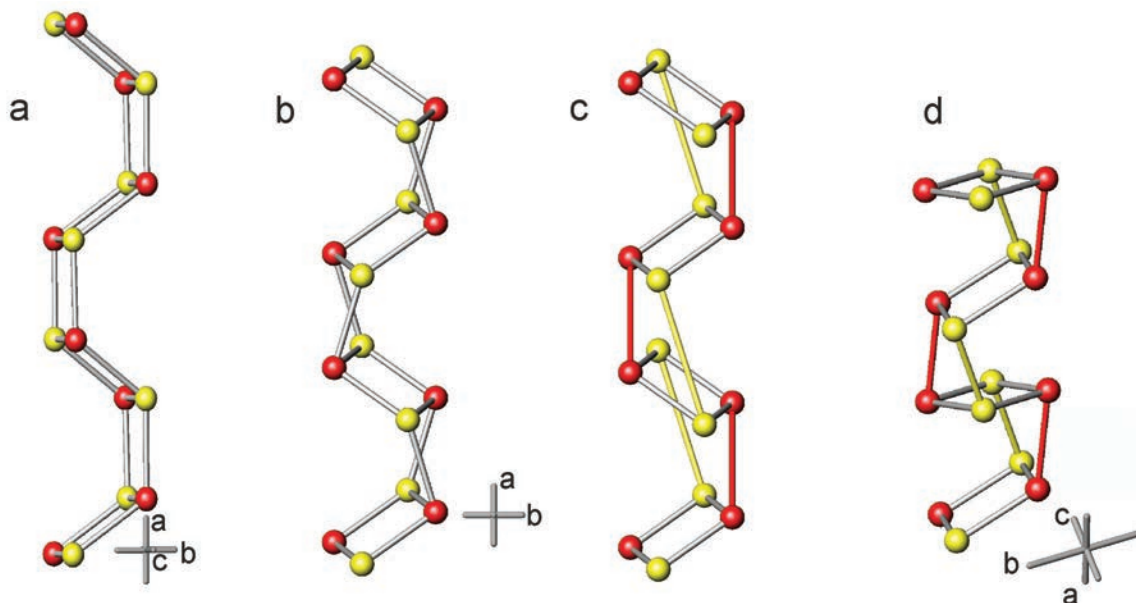


FIGURE 5. Model corresponding to Figure 4 but only a single double crankshaft is shown in a projection approximately perpendicular to the ones in Figure 4. (a) Chain in gismondine, space group $P2_1/c$ at 25 °C; (b) twisted chain in gismondine of space group $I2/a$ at 225 °C; (c) same chain as in b, but T-T connections approximately parallel to **a** are ruptured and new connections between tetrahedral centers of the same color are drawn. This example explains the topotactic transformation from a twisted **GIS** framework to a novel type of Ca feldspar structure with ordered Al-O-Al and Si-O-Si pairs shown in **d**.

according path II the Ca feldspar structure contracted by 26% compared to original gismondine (Fig. 2). As a consequence the newly formed Ca feldspar broke to several fragments; each twinned and yielding strongly broadened diffraction spots. Thus, a systematic search for possible superstructure reflections had to be abandoned. Nevertheless, we reject the hypothesis that the derived Si,Al order pattern is an artifact for the following reasons. (1) The strongly twisted double crankshaft chains in the partly dehydrated structure of gismondine (HT $I2/a$) leading to rupture of T-O-T bonds and development of new T-O-T linkages already suggested the observed unusual Si,Al order pattern. Consequently, the result of the structure study of the novel type of Ca feldspar confirmed the topotactic transformation model from gismondine to Ca feldspar. (2) As discussed above, all interatomic distances are in qualitative agreement with the described Si,Al order model. (3) We tested the influence of neglecting weak superstructure reflections for an anorthite from Monte Somma (Italy). A standard X-ray data collection resulted in a $P\bar{1}$ structure that is in agreement with findings of Angel et al. (1990). This structure shows essentially complete Si,Al order. Each oxygen is bonded to one Si and one Al. The mean T-O bonds of the eight SiO_4 tetrahedra vary between 1.617 and 1.622 Å and those of the eight AlO_4 tetrahedra between 1.739 and 1.751 Å. In the second step, all reflections below $50 I/\sigma(I)$, sensitive of Si,Al order, were removed thus the number of unique reflections halved from the original 10006 to 4992. The cell volume of the truncated data set of $P\bar{1}$ symmetry also halved and this average structure had 8 symmetry independent tetrahedra with average T-O distances between 1.678 and 1.689 Å. These average T-O distances are in line with averages obtained from

disorder of 50% Si and 50% Al in the center of the TO_4 unit. These average T-O distances were significantly different to those obtained for the unusual Si,Al order pattern in the Ca feldspar formed by dehydration of gismondine. In spite of the poor data quality, the novel Ca feldspar structure yielded similar average T-O bond lengths as found for pure SiO_4 and AlO_4 tetrahedra of Monte Somma anorthite.

Reinterpretation of van Reeuwijk's (1971) temperature dependent gismondine powder diffraction data

Van Reeuwijk (1971) displayed gismondine powder diffraction data up to 450 °C, but he used this information only to track structural changes and not to identify various structure types or their modifications. His powder data were contaminated by chabazite (main peak 001 at $d = 9.358$ Å), showed two Pt reflections (111, $d = 2.266$ and 002, $d = 1.9621$ Å) from the sample grid and four corundum reflections (at RT: 012, $d = 3.481$ Å; 014, $d = 2.551$ Å; 110, $d = 2.380$; and 113, $d = 2.086$ Å) used as internal standard. From all refined phases obtained in our gismondine dehydration study we produced CIF files¹, which were subsequently applied to calculate $\text{CuK}\alpha$ powder diffraction patterns imaged as film stripes. After appropriate scaling, these reference stripes were overlain on the diffraction film published by van Reeuwijk (1971). In general a **GIS** type framework produces a strong peak at about 7 Å. For fully hydrated gismondine at room temperature this diffraction maximum is at 7.28 Å, which shifts upon partial dehydration to 7.1 Å at 70 °C. The 75 °C pattern is in agreement with the three-phase assemblage: LT $P2_12_12_1$, LT $I2/a$, and reflections of an additional unknown **GIS** phase. Reflections of all three phases

fade at ca. 120 °C. At this temperature the GIS characteristic low-angle reflection shifts discontinuously to 6.6 Å accompanied by appearance of the HT $P2_12_12_1$ phase vanishing at ca. 200 °C. Together with the HT $P2_12_12_1$ phase we also observed reflections of the HT $I2/a$ phase, which fade at ca. 270 °C in favor of first occurrence of smeared Ca feldspar reflections. At 200 °C, the 6.6 Å peak becomes doubled by a second reflection at slightly higher d value, which persists until ca. 350 °C. This second GIS characteristic diffraction line is accompanied with a set of strong newly occurring reflections. We have no data for the GIS phase associated with these reflections but it seems that it is identical to phase D monitored by Milazzo et al. (1998) above 205 °C. Disappearance of reflections at 350 °C assigned to this D phase indicates a breakdown of the GIS framework and predominance of a Ca feldspar structure characterized by major intensities close to $d = 3.18$ Å.

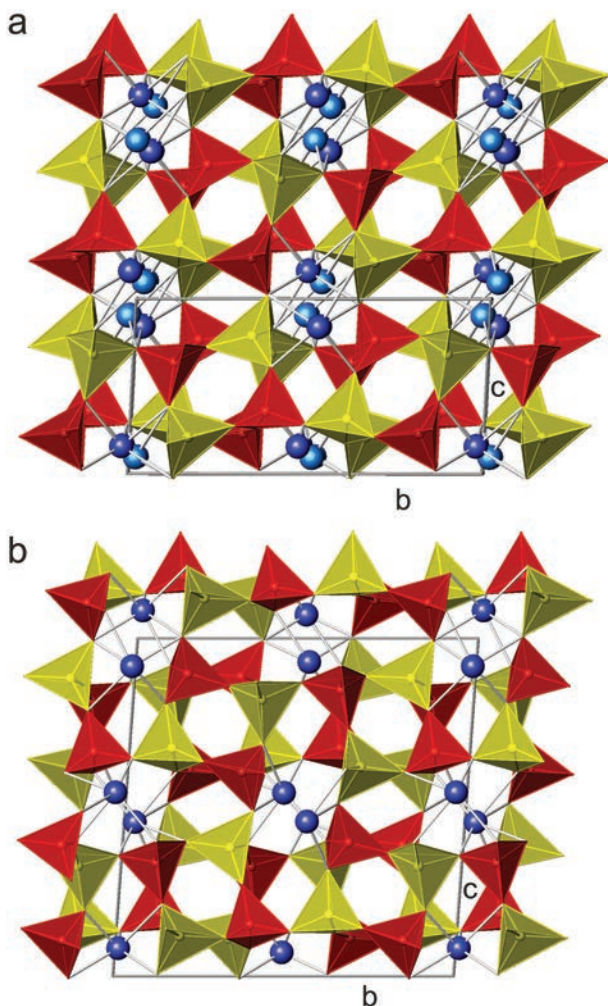


FIGURE 6. Comparison of the novel Ca feldspar structure with ordered Al-O-Al and Si-O-Si pairs occurring along the projection direction (a) with the conventional anorthite structure (b) with alternating Si and Al tetrahedra (Wainwright and Starkey 1971). The volume of the novel Ca feldspar unit cell is half of that of anorthite. Colors as in Figures 1 and 3.

For us, the most striking result of this reinterpretation is the strong evidence of coexistence of the phase LT $P2_12_12_1$ with LT $I2/a$ and HT $P2_12_12_1$ with HT $I2/a$, which means concurrent pathways I and II. This may also explain the low refinement quality of the LT $P2_12_12_1$ and HT $P2_12_12_1$ structures in our study. Corresponding lists of most disagreeing reflections displayed the general pattern that F_{obs} values were larger than F_{calc} indicating the possibility of an intimately intergrown second phase of GIS type, which was not recognized and could therefore not be separated based on the diffraction pattern. Concomitant occurrence of $P2_12_12_1$ and $I2/a$ GIS frameworks supports the hypothesis that both varieties are energetically very similar. The breakdown of the HT $I2/a$ phase is followed by first Ca feldspar formation at 270 °C, corresponding to 250 °C for path II in our study. This underlines the importance of the $I2/a$ phase as precursor of the novel Ca feldspar. In contrast, Milazzo et al. (1998) did not observe any evidence for phases according to our path II, and report thermal stability of the GIS phase D up to at least 440 °C without any evidence of Ca feldspar formation.

ACKNOWLEDGMENTS

The help of Biljana Lazic in the experimental part is highly appreciated. Frank Gfeller is acknowledged for producing film powder-diffraction images from CIF files. This study was supported by the Swiss National Science Foundation, grant "Crystal Chemistry of Minerals" 200020_134617 to T.A. and B.L. This paper benefitted from discussion with Rosa Micaela Danisi and Anna Pakhomova.

REFERENCES CITED

- Alberti, A., and Martucci, A. (2011) Reconstructive phase transitions in microporous materials: Rules and factors affecting them. *Microporous Mesoporous Materials*, 141, 192–198.
- Angel, R.J., Carpenter, M.A., and Finger, L.W. (1990) Structural variation associated with compositional variation and order-disorder behavior in anorthite-rich feldspars. *American Mineralogist*, 75, 150–162.
- Armbuster, T., and Gunter, M.E. (2001) Crystal structures of natural zeolites. In D. Bish, and D. Ming, Eds., *Natural Zeolites*, vol. 45, p. 1–67. Reviews in Mineralogy and Geochemistry, Mineralogical Society of America, Chantilly, Virginia.
- Artioli, G., Rinaldi, R., Kvik, Å., and Smith, J.V. (1986) Neutron diffraction structure refinement of the zeolite gismondine at 15K. *Zeolites*, 6, 361–366.
- Barth, T.F.W. (1935) Non-silicates with cristobalite-like structure. *Journal of Chemical Physics*, 3, 323–325.
- Bauer, T., and Baur, W.H. (1998) Structural changes in the natural zeolite gismondine (GIS) induced by cation exchange with Ag, Cs, Ba, Li, Na, K and Rb. *European Journal of Mineralogy*, 10, 133–147.
- Bruker (2009) Apex2 v. 2009–11.0 software package. Bruker AXS Inc., Madison, Wisconsin, U.S.A.
- Bruno, E., Chiari, G., and Facchinelli, A. (1976) Anorthite quenched from 1530 °C. I. Structure refinement. *Acta Crystallographica*, B32, 3270–3280.
- Büsem, W., and Eitel, A. (1936) Die Struktur des Pentacalciumaluminats. *Zeitschrift für Kristallographie*, 95, 175–188.
- Coombs, D.S., Alberti, A., Armbuster, T., Artioli, G., Colella, C., Galli, E., Grice, J.D., Liebau, F., Mandarino, J.A., Minato, H., and others. (1997) Recommended nomenclature for zeolite minerals: Report of the Subcommittee on zeolites of the International Mineralogical Association, Commission on New Minerals and Mineral Names. *Canadian Mineralogist*, 35, 1571–1606.
- Cortesogno, L., Lucchetti, G., and Penco, A.M. (1975) Associazioni a zeolite nel "Gruppo di Voltri": caratteristiche mineralogiche e significato genetico. *Rendiconti Società Italiana di Mineralogia e Petrologia*, 31, 673–710.
- Cruciani, G. (2006) Zeolites upon heating: factors governing their thermal stability and structural changes. *Journal of Physics and Chemistry of Solids*, 67, 1973–1994.
- Danisi, R.M., Armbuster, T., and Lazic, B. (2012) In situ dehydration behavior of zeolite-like cavansite: A single-crystal X-ray study. *American Mineralogist*, 97, 1874–1880.
- (2013) In situ dehydration behavior of zeolite-like pentagonite: A single-crystal X-ray study. *Journal of Solid State Chemistry*, 197, 508–516.
- Fischer, K.F. (1963) The crystal structure determination of zeolite gismondite $\text{CaAl}_2\text{Si}_2\text{O}_8 \cdot 4\text{H}_2\text{O}$. *American Mineralogist*, 48, 664–672.
- Galuskin, E.V., Kusz, J., Armbuster, T., Bailau, R., Galuskina, I.O., Ternes, B., and Murashko, M. (2012) A reinvestigation of mayenite from the type locality, the Ettringer Bellerberg volcano near Mayen, Eifel district, Germany. *Mineralogical*

- cal Magazine, 76, 707–716.
- Kimata, M., and Ii, N. (1984) The structural property of synthetic gehlenite, $\text{Ca}_2\text{Al}_2\text{SiO}_7$. *Neues Jahrbuch für Mineralogie, Abhandlungen*, 144, 254–267.
- Lazic, B., Armbruster, T., Liebich, B.W., and Perfler, L. (2012) Hydrogen-bond system and dehydration behavior of the natural zeolite parthéite. *American Mineralogist*, 97, 1866–1873.
- Loewenstein, W. (1954) The distribution of aluminium in the tetrahedra of silicates and aluminates. *American Mineralogist*, 39, 92–96.
- Meier, W.M. (1968) Zeolite structures. In *Molecular Sieves*, p. 10–27. Society of Chemical Industry, London.
- Milazzo, E., Artioli, G., Gualtieri, A., and Hanson, J.C. (1998) The dehydration process in gismondine: An in situ Synchrotron XRPD study. *Proceedings IV Convegno Nazionale Scienza e Tecnologia delle Zeoliti*, 160–165.
- Rinaldi, R., and Vezzalini, G. (1985) Gismondine: the detailed X-ray structure refinement of two natural samples. In B. Drzaj, Hocevar, S., and Pejovnik, S., Eds., *Zeolites*, p. 481–492. Elsevier, Amsterdam.
- Sahl, K. (1980) Refinement of the crystal structure of bicchulite, $\text{Ca}_2[\text{Al}_2\text{SiO}_6](\text{OH})_2$. *Zeitschrift für Kristallographie*, 152, 13–21.
- Sheldrick, G.M. (2008) A short history of SHELX. *Acta Crystallographica*, A64, 112–122.
- Smith, J.V. (1968) Further discussion of framework structures built from four- and eight-membered rings. *Mineralogical Magazine*, 36, 640–642.
- Smith, J.V., and Rinaldi, F. (1962) Framework structures from parallel four- and eight-membered rings. *Mineralogical Magazine*, 33, 202–212.
- Van Reeuwijk, L.P. (1971) The dehydration of gismondite. *American Mineralogist*, 56, 1655–1659.
- Vezzalini, G., Quartieri, S., and Alberti, A. (1993) Structural modifications induced by dehydration in the zeolite gismondine. *Zeolites*, 13, 34–42.
- Vezzalini, G., Alberti, A., Sani, A., and Triscari, M. (1999) The dehydration process in amicitite. *Microporous and Mesoporous Materials*, 31, 253–262.
- Wadoski, E., Armbruster, T., Lazic, B., and Fisch, M. (2011) Dehydration of the natural zeolite goosecreekite $\text{CaAl}_2\text{Si}_6\text{O}_{16} \cdot 5\text{H}_2\text{O}$ upon stepwise heating: A single-crystal and powder X-ray study. *American Mineralogist*, 96, 1070–1078.
- Wainwright, J.E., and Starkey, J. (1971) A refinement of the structure of anorthite. *Zeitschrift für Kristallographie*, 133, 75–84.

MANUSCRIPT RECEIVED FEBRUARY 5, 2013

MANUSCRIPT ACCEPTED JUNE 18, 2013

MANUSCRIPT HANDLED BY G. DIEGO GATTA